

# Effect of Alloying Elements on the Stacking Fault Energy and Ductility in $Mg_2Si$ Intermetallic Compounds

Xinpeng Zhao, Keke Song, Haiyou Huang,\* Yu Yan, Yanjing Su, and Ping Qian

Cite This: *ACS Omega* 2021, 6, 20254–20263

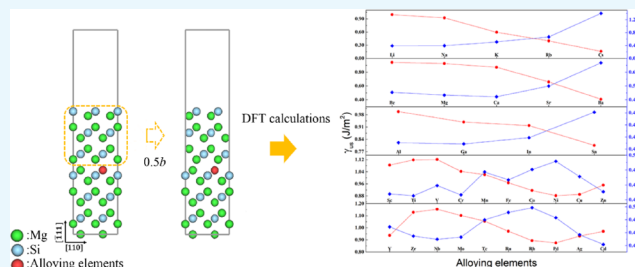
Read Online

ACCESS |

Metrics &amp; More

Article Recommendations

**ABSTRACT:** Alloying elements can pronouncedly change the mechanical properties of intermetallic compounds. However, the effect mechanism of this in  $Mg_2Si$  alloys is not clear yet. In this paper, systematic first-principles calculations were performed to investigate the effect of alloying elements on the ductility of Mg–Si alloys. It was found that some alloying elements such as In, Cu, Pd, etc. could improve the ductility of  $Mg_2Si$  alloys. Moreover, the interatomic bonding mechanisms were analyzed through the electron localization functional. Simultaneously, the machine-learning method was employed to help identify the most important features associated with the toughening mechanisms. It shows that the ground state atomic volume ( $V_{GS}$ ) is strongly related to the stacking fault energy ( $\gamma_{us}$ ) of  $Mg_2Si$  alloys. Interestingly, the alloying elements with appropriate  $V_{GS}$  and higher Allred–Rochow electronegativity ( $En$ ) would reduce the  $\gamma_{us}$  in the Mg–Si–X system and yield a better ductility. This work demonstrates how a fundamental theoretical understanding at the atomic and electronic levels can rationalize the mechanical properties of  $Mg_2Si$  alloys at a macroscopic scale.



## 1. INTRODUCTION

Magnesium (Mg) alloys are one of the development directions of structural and functional materials in the present and will be in the future due to their good damping capacity, low density, high strength-to-weight ratio, and biodegradability. The intermetallic compound of  $Mg_2Si$  is a promising thermoelectric material because of its high thermoelectric performance.<sup>1–5</sup> In addition,  $Mg_2Si$  also has excellent hydrogenation properties, making it one of the candidates for hydrogen storage materials.<sup>6</sup> Due to a narrow band gap of about 0.6 eV,  $Mg_2Si$  can be used as an infrared detector operating in the 1.2–2.0  $\mu m$  wavelength range.<sup>7</sup> Meanwhile, nontoxicity, low production cost, and huge thermoelectric conversion efficiency of  $Mg_2Si$  are required for its successful commercialization. These features make  $Mg_2Si$  suitable for a variety of applications, including the automotive and aerospace industries. Unfortunately,  $Mg_2Si$  alloys show very low ductility and strength.

Therefore, designing novel Mg–Si alloys with improved ductility has become critically important.  $Mg_2Si$  has a face-centered cubic (FCC)  $CaF_2$ -type crystal structure, which possesses sufficient possible dislocation slip systems. In the previous study, we demonstrated that the strong covalent bond characteristic of the Si atom is the primary reason for its brittleness.<sup>8</sup> There are two main approaches to improve ductility. An effective approach is to refine the grain size, which can enhance the formability of alloys.<sup>9–11</sup> However, the expensive refining process increases the material cost. Another

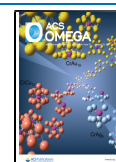
approach is to introduce alloying elements. The addition of certain alloying elements to a metal is one of the most effective ways of altering the local structure and chemistry of alloys,<sup>12</sup> and it can also be used to improve the ductility and fracture toughness of the alloy.<sup>13</sup> For example, Qu and co-workers improved the room-temperature ductility of TiAl by adding the La element.<sup>14</sup> Alloying can also change the anisotropy of electron distribution around Al atoms that could influence the slip behavior in pure aluminum.<sup>15</sup> For  $Mg_2Si$  alloys, at present, Al addition plays a critical role in increasing the ductility of  $Mg_2Si$ .<sup>8</sup> Another research indicates that doping In, Li, Sn, and Bi can efficiently improve the ductility of Mg alloys.<sup>16</sup> However, the understanding of the effect of alloying elements on  $Mg_2Si$  alloys is still far from sufficient and a great deal of effort is required to find ideal alloying elements.

Actually, it is difficult to directly measure the effect of alloying elements on important features such as the resultant changes in the chemical environment at a boundary. As a result, the calculation approaches based on density functional theory (DFT) have been used to predict the mechanical

Received: April 20, 2021

Accepted: July 19, 2021

Published: July 28, 2021



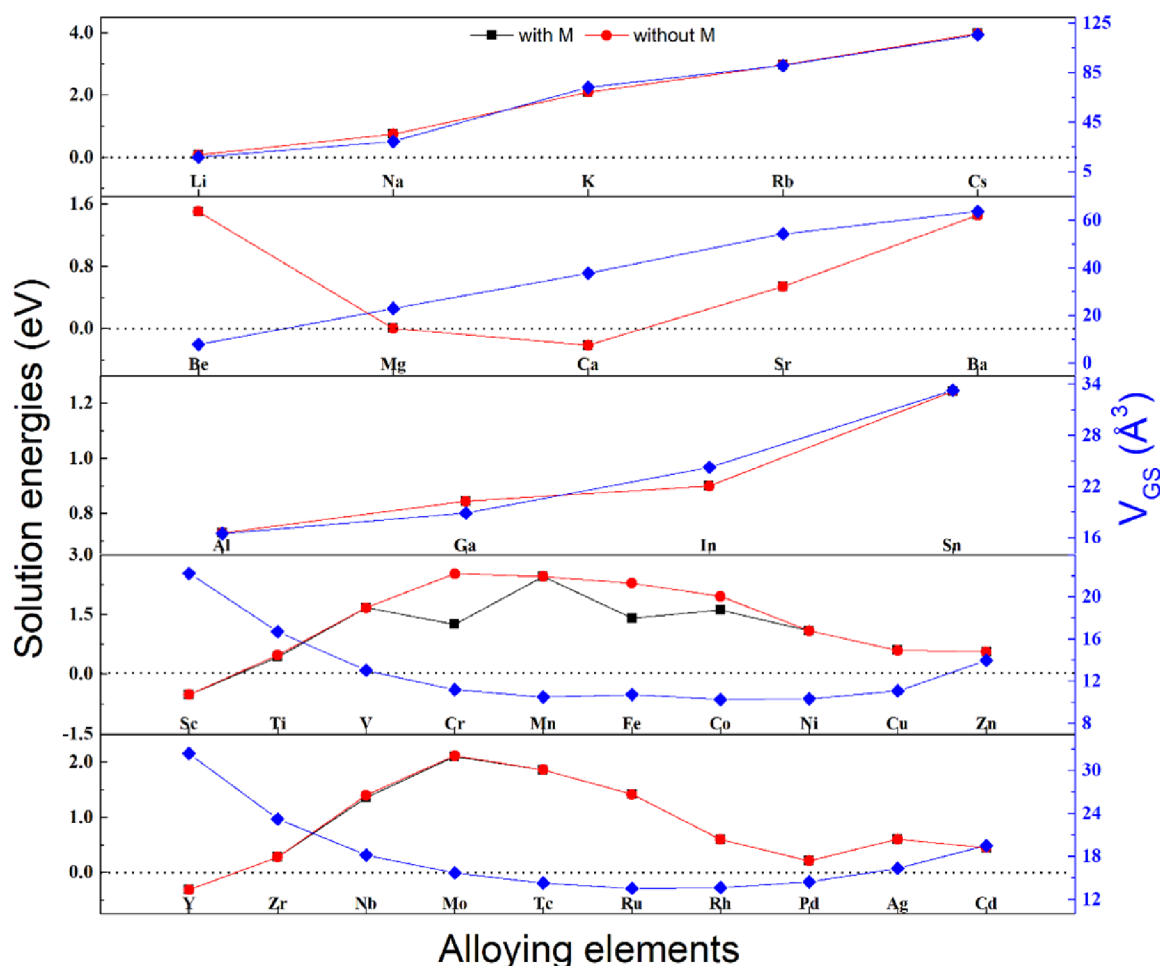


**Figure 1.** Solution energies of alloying elements in  $\text{Mg}_2\text{Si}$ . The red circles and black squares represent the magnetic character of the element that was considered or not, respectively. The blue rhombuses represent the  $V_{\text{GS}}$  of the alloying elements.

properties of Mg alloys. A design map of Mg alloys based on the intrinsic ductility was established by DFT.<sup>17</sup> The stacking fault energy (SFE) is a critical intrinsic material parameter that significantly affects plastic deformation behavior and mechanical properties. Wu *et al.* found that the dominant factor in the reduction of SFE is the charge redistribution surrounding the alloying elements.<sup>18</sup> Tsuru *et al.* showed distinctive hybridization between the  $p$  band of Mg and the  $d$  band of the alloying element, which characterizes the strong fracture toughness of Mg-based binary alloys.<sup>19</sup> Therefore, comprehensive DFT calculations can certainly help us understand the important features and the mechanism in  $\text{Mg}_2\text{Si}$  alloys.

In the present work, we introduced the SFE to understand the effect of alloying elements on the ductility of Mg–Si alloys. We chose the  $\{111\}\langle 110 \rangle$  habit slip system because it is the habit slip system for FCC metals. Then, extensive DFT calculations were performed to reveal the general trends of the energetic properties of a large number of alloying elements across the periodic table doping to the slip plane in the FCC  $\text{Mg}_2\text{Si}$  matrix. For possible alloying elements, we considered 33 elements including five elements from group I (i.e., Li, Na, K, Rb, and Cs), four elements from group II (i.e., Be, Ca, Sr, and Ba), four elements from groups III and IV (i.e., Al, Ga, In and Sn), and all 3d and 4d transition metals (TMs). Following that, we also unraveled the intrinsic microscopic electronic mechanism of  $\text{Mg}_2\text{Si}$  alloys doped with alloying elements.

Finally, the effects of possible factors on the variations of SFE in  $\text{Mg}_2\text{Si}$  were investigated by machine learning (ML) due to its advantage in effectively finding features related to performance.<sup>20–22</sup> The results of this study can provide a theoretical reference for alloying design of multicomponent Mg–Si alloys.

## 2. RESULTS AND DISCUSSION

**2.1. Solution Energy.** The solution energy ( $E_{\text{sol}}$ ) can be described by<sup>23</sup>

$$E_{\text{sol}} = E_{\text{tot}}^{\text{Mg-Si-X}} - \sum_i n_i E_i^{\text{bulk}} \quad (1)$$

where  $E_{\text{tot}}^{\text{Mg-Si-X}}$  is the total energy of the alloying-element-doped  $\text{Mg}_2\text{Si}$  supercells,  $n_i$  is the atom number of each element in the supercell, and  $E_i^{\text{bulk}}$  denotes the energy per atom of each element in the stable ground state. The alloying element can be alloyed into the  $\text{Mg}_2\text{Si}$  system spontaneously if the solution energy  $E_{\text{sol}}$  is negative. The more negative the  $E_{\text{sol}}$  is, the more likely it will appear.

The calculated equilibrium lattice parameter of undoped FCC  $\text{Mg}_2\text{Si}$  was 0.636 nm. This result is in good agreement with the experimental value of 0.635 nm.<sup>24</sup> The solution energies of alloying elements in  $\text{Mg}_2\text{Si}$  were calculated by considering the magnetic moment of these alloying elements during the electronic self-consistent calculation. Since the

Table 1. SFE in Mg–Si–X Systems, Together with Properties of Mg<sub>2</sub>Si Alloys Doped with Alloying Elements<sup>a</sup>

alloying elements	$E_{\text{sol}}$ (with M) (eV)	$E_{\text{sol}}$ (without M) (eV)	$\gamma_{\text{us}}$ (J/m <sup>2</sup> )	$\gamma_{\text{s}}$ (J/m <sup>2</sup> )	$D$	$V_{\text{GS}}$ (Å <sup>3</sup> )	En
Li	0.078	0.078	0.997	1.297	0.390	16.59	0.97
Be	1.499	1.500	0.942	1.425	0.454	7.89	1.47
Na	0.742	0.742	0.924	1.215	0.395	29.24	1.01
Mg	0.000	0.000	0.925	1.336	0.433	22.89	1.23
Al	0.729	0.729	0.998	1.415	0.425	16.48	1.47
K	2.089	2.089	0.595	1.015	0.511	73.11	0.91
Ca	-0.215	-0.215	0.872	1.225	0.422	37.77	1.04
Sc	-0.519	-0.519	1.084	1.502	0.416	22.24	1.20
Ti	0.430	0.474	1.118	1.531	0.411	16.69	1.32
V	1.665	1.665	1.121	1.637	0.438	13.01	1.45
Cr	1.253	2.518	1.042	1.436	0.413	11.19	1.56
Mn	2.452	2.451	1.021	1.616	0.475	10.49	1.60
Fe	1.403	2.285	0.968	1.463	0.454	10.73	1.64
Co	1.608	1.951	0.916	1.470	0.481	10.25	1.70
Ni	1.089	1.089	0.882	1.479	0.503	10.32	1.75
Cu	0.590	0.590	0.890	1.371	0.462	11.07	1.75
Zn	0.562	0.562	0.951	1.337	0.422	13.96	1.66
Ga	0.844	0.844	0.938	1.327	0.424	18.86	1.82
Rb	2.966	2.966	0.398	0.884	0.667	90.72	0.89
Sr	0.540	0.540	0.659	1.095	0.499	54.23	0.99
Y	-0.321	-0.321	0.937	1.429	0.458	32.37	1.11
Zr	0.279	0.279	1.128	1.614	0.429	23.20	1.22
Nb	1.360	1.401	1.154	1.612	0.419	18.18	1.23
Mo	2.105	2.117	1.101	1.564	0.426	15.69	1.30
Tc	1.861	1.861	1.055	1.686	0.479	14.29	1.36
Ru	1.417	1.417	0.972	1.628	0.503	13.51	1.42
Rh	0.597	0.597	0.894	1.541	0.517	13.64	1.45
Pd	0.210	0.210	0.875	1.418	0.486	14.41	1.35
Ag	0.602	0.602	0.931	1.345	0.433	16.33	1.42
Cd	0.447	0.447	0.971	1.306	0.403	19.50	1.46
In	0.899	0.899	0.918	1.314	0.429	24.26	1.49
Sn	1.244	1.243	0.806	1.210	0.451	33.29	1.72
Cs	3.971	3.971	0.159	0.742	1.397	115.77	0.86
Ba	1.454	1.454	0.408	0.907	0.667	63.59	0.97

<sup>a</sup>Properties of Mg–Si–X systems are the solution energy ( $E_{\text{sol}}$ ) with the initial magnetic character being considered or not. The SFE, cleavage free surface energy, and ductility parameter are noted as  $\gamma_{\text{us}}$ ,  $\gamma_{\text{s}}$ , and  $D$ , respectively. Two features of alloying elements of ground state atomic volume ( $V_{\text{GS}}$ ) and Allred–Rochow electronegativity (En) are also listed.

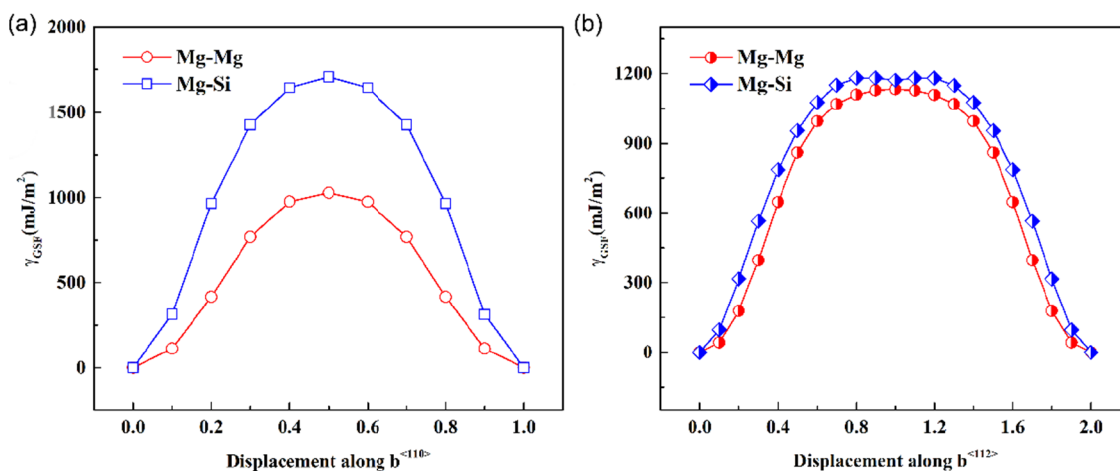
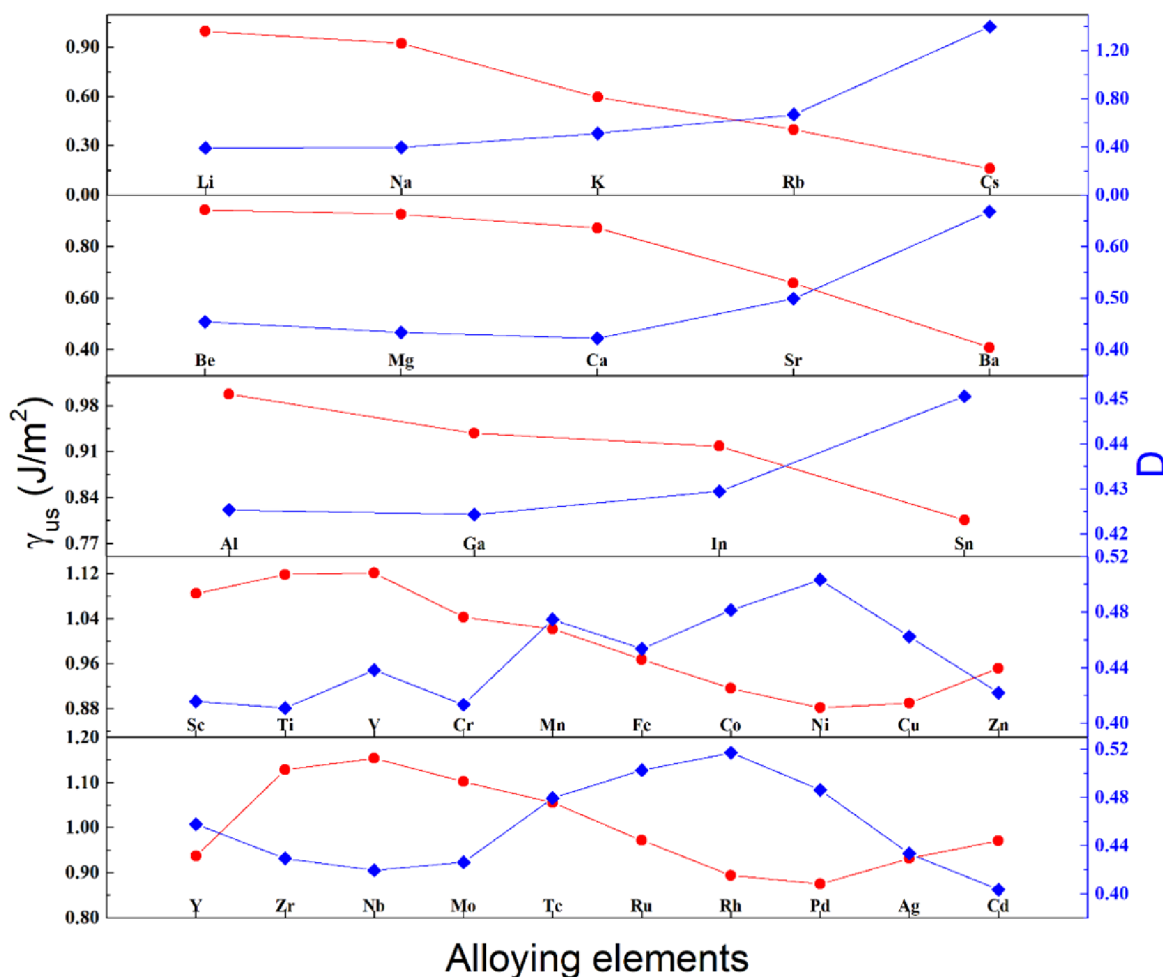


Figure 2. First-principles calculated GSF curves of pure Mg<sub>2</sub>Si along the (a)  $\langle 110 \rangle$  and (b)  $\langle 112 \rangle$  directions.

lattice distortion will cause the system energy change when the alloy element atomic size difference is large, we consider the influence of the ground state atomic volume ( $V_{\text{GS}}$ ) on the  $E_{\text{sol}}$ . As shown in Figure 1 and Table 1, the solution energies have a

strong correlation with the  $V_{\text{GS}}$ . The alloying elements of groups I, II, III, and IV have the same trend that as  $V_{\text{GS}}$  increases, the solution energy increases. On the contrary, for all 3d- and 4d-TM alloying elements, it is observed that the



**Figure 3.** Effects of alloying elements on the SFE and ductility of  $\text{Mg}_2\text{Si}$ . The red circles and blue rhombuses represent the SFE and  $D$  of the alloying elements, respectively.

solution energies and  $V_{\text{GS}}$  have a negative correlation. Alloying elements are easier to insert on the Mg site in  $\text{Mg}_2\text{Si}$  if their  $V_{\text{GS}}$  values are similar to those of Mg. After the electronic self-consistent calculations, it is found that the magnetic character of the initially set magnetic alloying elements Ti, Cr, Fe, Co, Nb, and Mo still exists, while other systems become nonmagnetic. Therefore, in the following calculations, only the magnetism of the alloying elements Ti, Cr, Fe, Co, Nb, and Mo is considered.

**2.2. Generalized SFE of  $\text{Mg}_2\text{Si}$ .** The generalized SFE (GSFE) is expressed as<sup>18</sup>

$$\gamma_{\text{GSF}} = \frac{E_f - E_p}{S} \quad (2)$$

where  $E_f$  is the total energy of the stacked configuration with the fault vector  $\mathbf{u}$ .  $E_p$  is the total energy of the stacked configuration without slipping.  $S$  is the faulted area of the supercell.

In the Mg–Si system, there are two types of slip planes, the Mg–Mg plane and Mg–Si plane. Each slip plane has two possible slip systems, the  $\{111\}\langle 112 \rangle$  slip system and  $\{111\}\langle 110 \rangle$  slip system. Figure 2 presents the GSFE curves of all slip systems for the undoped  $\text{Mg}_2\text{Si}$ . The maximum energy on the GSFE curve is the unstable SFE ( $\gamma_{\text{us}}$ ), which determines the energy barrier for the nucleation of trailing dislocations. It occurs around  $0.8b^{(112)}$  and  $0.5b^{(110)}$  for the

Mg–Si plane and at  $b^{(112)}$  and  $0.5b^{(110)}$  for the Mg–Mg plane. The Burgers vectors are  $b^{(112)} = (1/6)\langle 112 \rangle a_0$  and  $b^{(110)} = (1/6)\langle 110 \rangle a_0$ . The GSFE curves indicate that the  $\gamma_{\text{us}}$  of the Mg–Mg plane along the  $\langle 110 \rangle$  direction is lower than that along the  $\langle 112 \rangle$  direction, while the  $\gamma_{\text{GSF}}$  of the Mg–Si plane is opposite. The Mg–Mg plane exhibits a lower  $\gamma_{\text{us}}$  compared to the Mg–Si plane in both slip directions. So, the  $\langle 110 \rangle$  direction on the Mg–Mg plane is the slip system in the  $\text{Mg}_2\text{Si}$  alloy.

**2.3. Alloying Effect of X on the Ductility of  $\text{Mg}_2\text{Si}$ .** The ductility can be predicted by the ductility parameter  $D$ . It is the ratio of the cleavage free surface energies  $\gamma_s$  to the unstable SFEs  $\gamma_{\text{us}}$ . An increased value of  $D$  represents an enhancement of ductile tendency. The ductility parameter  $D$  is defined as<sup>25</sup>

$$D = \frac{0.3\gamma_s}{\gamma_{\text{us}}} \quad (3)$$

The cleavage free surface energy  $\gamma_s$  is given by<sup>26</sup>

$$\gamma_s = \frac{E_{\text{half}}^{\text{FS1}} + E_{\text{half}}^{\text{FS2}} - E_p}{S} \quad (4)$$

where  $E_{\text{half}}^{\text{FS1}}$  and  $E_{\text{half}}^{\text{FS2}}$  represent the total energies of two half slabs, respectively.

The effects of alloying elements on the SFE and ductility of  $\text{Mg}_2\text{Si}$  are shown in Figure 3 and also listed in Table 1. The

alloying elements of groups I, II, III, and IV have the same trend that as  $\gamma_{\text{us}}$  decreases, the  $D$  increases, indicating that there is an increasing tendency of ductility. This trend can be seen clearly in the  $\gamma_{\text{us}}$  for a given alloying element.

The variation of  $\gamma_{\text{us}}$  with respect to the 3d- and 4d-TMs alloying elements seems to be more complicated and follows a concave-up parabolic-like dependency, which is distorted at the right end. Moving to the right of the periodic table,  $\gamma_{\text{us}}$  tends to increase slightly and peaks at V and Nb where it begins to decrease to its minimum at Ni and Pd. On the whole, the ductility seems to be worse for late TMs, in particular, those of columns 9 and 10. Finally, it is worth mentioning that our result  $D$  herein is also supported by previous experimental studies regarding the alloying effects on the ductile–brittle transition temperature of  $\text{Mg}_2\text{Si}$ .<sup>27</sup> In experimental studies, compared to Al and Ti, solution of Cu can effectively increase the ductility of  $\text{Mg}_2\text{Si}$ .

**2.4. Electron Localization Functional Analyses.** The effect of alloying elements on the interatomic bonding characteristics of slip planes can be studied in detail by the electron localization functional (ELF). The ELF is very important for an analysis of interatomic bonding mechanisms. We select five typical alloying elements, K from group I, Sr from group II, In from group III and IV, Cu from 3d-TMs, and Pd from 4d-TMs. They do not change the value of  $\gamma_{\text{s}}$  and decrease the value of  $\gamma_{\text{us}}$  in  $\text{Mg}_2\text{Si}$ . The ELF vertical slip planes of the five slip systems are depicted in Figure 4. The range of

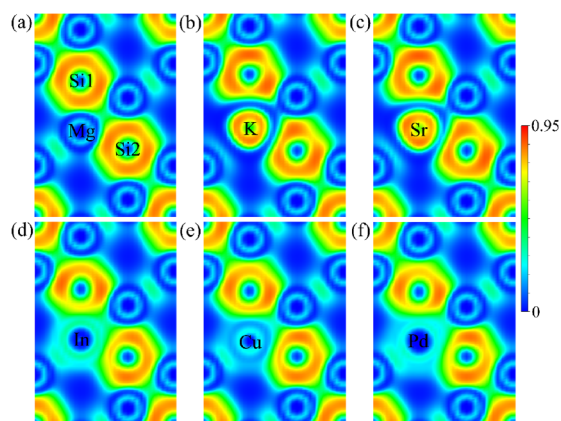


**Figure 4.** ELF images of (a) pristine and (b) K-, (c) Sr-, (d) In-, (e) Cu-, and (f) Pd-alloyed- $\text{Mg}_2\text{Si}$  systems in the (101) plane. The color scale is given at the right.

ELF is between 0 and 1, where 0 represents no bonding between the adjacent atoms, 0.5 represents a perfect metallic bond, and a higher ELF value indicates that the electrons are more localized (ELF = 1 can be interpreted as perfect localization). All ELF contour plots reveal similar chemical bonding characteristics and indicate that K, Sr, In, Cu, and Pd can weaken the nearest Si–Si bond (Si1–Si2 bond in Figure 4) in  $\text{Mg}_2\text{Si}$  alloys.

The ELF value on a line segment with equal steps can be calculated by linear integration of volumetric ELF data. The minimum ELF value in the middle of linear ELF represents the relative strength of bonding.<sup>28</sup> The effect of alloying elements on the SFE may be analyzed with the strength of neighboring Si1–Si2 bonds vertical to the slip plane. Further details can be seen in Figure 5, which shows that K, Sr, In, Cu, and Pd decrease the strength of neighboring Si1–Si2 bonds because

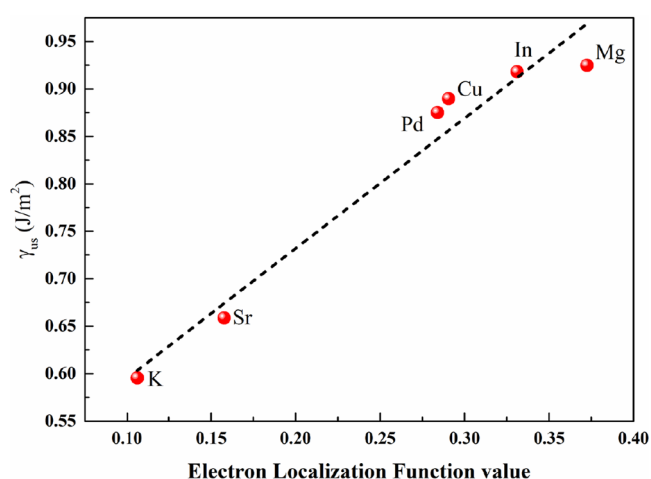


**Figure 5.** SFE of the different alloying elements as a function of the minimum ELF value in the middle of the Si1–Si2 bond.

the alloying elements deplete the electrons between Si1 and Si2 atoms. Moreover, due to the different electron attraction ability of alloying elements, the influence of the strength of neighboring Si1–Si2 bonds on the SFE presents a linear trend. The smaller the strength of neighboring Si1–Si2 bonds is, the lower the SFE is.

**2.5. Contributing Factors to SFE in Mg–Si–X systems.** To figure out possible factors that may contribute to the variations of SFE in Mg–Si–X alloying systems, we discuss here how we chose the relevant features that form the input to the ML model. A physical understanding of what kind of features affect SFE has been the basis to intuitively screen the alloying elements of alloys and has been widely discussed in literature studies.<sup>26,29,30</sup> Generally, alloying elements will affect the SFE of alloys as a result of two mechanisms, which are the size effect and the electronic effect.<sup>26</sup>

Several criteria are proposed to describe SFE in Mg–Si–X systems based on the accumulated energy ionization ( $E_{\text{ia}}$ ), the Allred–Rochow electronegativity ( $E_{\text{n}}$ ), the first ionization energy ( $E_{\text{i1}}$ ), the atomic number ( $A_{\text{num}}$ ), the covalent radius ( $R_{\text{cov}}$ ),<sup>31</sup> Clementi’s effective nuclear charge ( $Z_{\text{cle}}$ ), the valence electron concentration (VEC), Zunger’s pseudopotential radii ( $R_{\text{dor}}$ ), Brewer’s cohesive energy ( $E_{\text{c}}$ ),<sup>32</sup> the number of unfilled valence orbitals ( $N_{\text{val}}$ ), the energy per atom of the  $T = 0$  K ground state ( $E_{\text{GS}}$ ), the ground state atomic volume ( $V_{\text{GS}}$ ),<sup>33</sup> and the valence (val).<sup>34</sup> These features represent a coarse-grained analogue of radial and electronic properties in Mg–Si–X systems and provide a relatively simple physical basis for modeling the structure–property relationship for the SFE. Our final feature pool consists of 13 features. A detailed list of these features is provided in Table 2.

Random forest<sup>35–39</sup> is a popular and efficient model based on the decision tree, which has the ability to perform both regression and classification. We evaluate each feature according to the feature importance based on random forest regression (RFR). The higher the feature importance score is, the more important the feature is. The importance of a feature is computed as the (normalized) total reduction of the criterion brought by that feature. It is also known as the Gini importance. As shown in Figure 6,  $V_{\text{GS}}$  demonstrated the highest level of importance. Moreover, it can be seen that the feature importance of the size effect ( $V_{\text{GS}}$ ,  $R_{\text{cov}}$ , and  $R_{\text{dor}}$ ) is relatively high, which indicates that the size effect is the main

Table 2. Thirteen Physical Features of Different Alloying Elements for ML Modeling

alloying elements	$E_{ia}$ (eV)	En	$Z_{cle}$	$E_{il}$ (kJ/mol)	$N_{val}$	$A_{num}$	VEC	val	$R_{cov}$ (pm)	$V_{GS}$ ( $\text{\AA}^3$ )	$R_{dor}$ (pm)	$E_c$ (eV)	$E_{GS}$ (eV/atom)
Li	204.185	0.97	1.28	520.22	1	3	1	1	133	16.59	161	1.63	-1.870
Be	182.046	1.47	1.91	899.50	0	4	2	2	102	7.89	108	3.32	-3.755
Na	124.486	1.01	2.51	495.85	1	11	1	1	155	29.24	265	1.11	-1.260
Mg	103.186	1.23	3.31	737.75	0	12	2	2	139	22.89	203	1.51	-1.542
Al	53.452	1.47	4.07	577.54	5	13	3	3	126	16.48	168	3.39	-3.745
K	81.960	0.91	3.50	418.81	1	19	1	1	196	73.11	369	0.93	-1.098
Ca	69.127	1.04	4.40	589.83	0	20	2	2	171	37.77	300	1.84	-1.948
Sc	44.252	1.20	4.63	633.09	9	21	3	3	148	22.24	275	3.90	-6.286
Ti	48.058	1.32	4.82	658.81	8	22	4	4	136	16.69	258	4.85	-7.775
V	50.880	1.45	4.98	650.91	7	23	5	5	134	13.01	243	5.31	-8.939
Cr	54.411	1.56	5.13	652.87	6	24	6	6	122	11.19	244	4.10	-9.506
Mn	56.934	1.60	5.23	717.28	5	25	7	4	119	10.49	222	2.92	-9.021
Fe	54.884	1.64	5.43	762.47	4	26	8	3	116	10.73	211	4.28	-8.285
Co	58.619	1.70	5.58	760.40	3	27	9	4	111	10.25	202	4.39	-7.080
Ni	61.180	1.75	5.71	737.14	2	28	10	2	110	10.32	218	4.44	-5.546
Cu	65.077	1.75	5.84	745.48	1	29	11	2	112	11.07	204	3.49	-3.681
Zn	67.313	1.66	5.97	906.40	0	30	12	2	118	13.96	188	1.35	-1.240
Ga	57.416	1.82	6.22	578.84	5	31	3	3	124	18.86	170	2.81	-3.012
Rb	71.698	0.89	4.98	403.03	1	37	1	1	210	90.72	410	0.85	-0.963
Sr	60.533	0.99	6.07	549.47	0	38	2	2	185	54.23	321	1.72	-1.683
Y	39.277	1.11	6.26	599.87	9	39	3	3	163	32.37	294	4.37	-6.465
Zr	43.108	1.22	6.45	640.10	8	40	4	4	154	23.20	283	6.25	-8.546
Nb	46.403	1.23	6.70	652.13	7	41	5	5	147	18.18	276	7.57	-10.093
Mo	50.585	1.30	6.98	684.32	6	42	6	6	138	15.69	272	6.82	-10.846
Tc	52.254	1.36	7.23	686.92	5	43	7	6	128	14.29	265	6.85	-10.355
Ru	52.781	1.42	7.45	710.18	4	44	8	6	125	13.51	261	6.74	-9.195
Rh	56.792	1.45	7.64	719.67	3	45	9	6	125	13.64	252	5.75	-7.254
Pd	60.910	1.35	7.84	804.38	0	46	10	4	120	14.41	245	3.89	-5.138
Ag	64.126	1.42	8.03	731.00	1	47	11	1	128	16.33	238	2.95	-2.765
Cd	63.593	1.46	8.19	867.77	0	48	12	2	136	19.50	222	1.16	-0.812
In	52.877	1.49	8.47	558.30	5	49	3	3	142	24.26	205	2.52	-2.667
Sn	52.661	1.72	9.10	708.58	4	50	4	4	140	33.29	188	3.14	-3.961
Cs	62.210	0.86	6.36	375.70	1	55	1	1	232	115.77	431	0.80	-0.855
Ba	52.145	0.97	7.58	502.85	0	56	2	2	196	63.59	340	1.90	-1.924

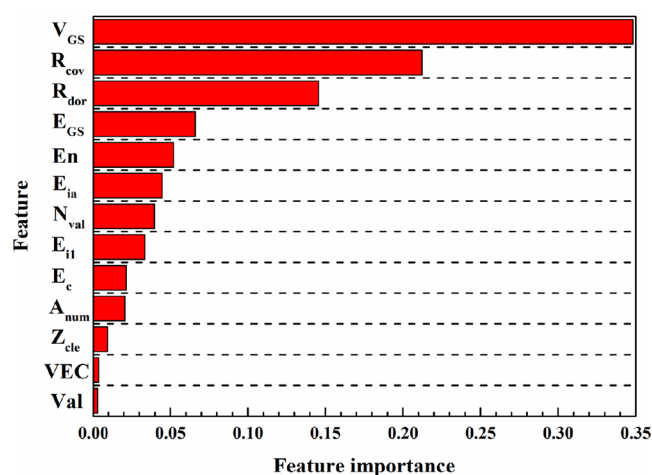


Figure 6. RFR-based feature importance of 13 features.

factor affecting the SFE of  $Mg_2Si$ . The importance of the electronic effect is relatively low, indicating that its influence on SFE is not as strong as that of the size effect.

The Pearson correlation coefficient is also chosen for evaluating the linear relationship between variables  $X$  and  $Y$

$$\text{corr}(X, Y) = \frac{\text{cov}(X, Y)}{\sigma_X \sigma_Y} \quad (5)$$

where  $\text{cov}(X, Y)$  represents the covariance between  $X$  and  $Y$  and  $\sigma_X$  and  $\sigma_Y$  represent the standard deviations for  $X$  and  $Y$ , respectively. The Pearson correlation coefficient varies from  $-1$  to  $1$ . The value of the coefficient is  $1/-1$ , which indicates a perfect linear positive/negative correlation between  $X$  and  $Y$ . The value of the coefficient is  $0$ , which means that there is no linear relationship between the two variables.

Multiple correlation matrices between  $\gamma_{us}$  and 13 features of alloying elements were computed, as shown in Figure 7. The correlation coefficient  $\text{cov}(\gamma_{us}, V_{GS}) = -0.90$  was used. It should be noted that the absolute correlation coefficient value of  $0.90$  indicates a strong relationship between  $\gamma_{us}$  and  $V_{GS}$ . As a consequence, the most possible feature that contributes to SFE is  $V_{GS}$ . Other features of the electronic effect have a relatively low correlation with  $\gamma_{us}$  compared to  $V_{GS}$ . This is consistent with the above feature importance results. It is worth mentioning that both solution energy and SFE have a strong correlation with  $V_{GS}$ . Similarly,  $V_{GS}$  may also affect other properties of the alloy. Therefore, the size effect should be one of the most important features in alloy design.

**2.6. Statistical Analysis.** A visual representation of the relationship between  $\gamma_{us}$  and the most contributing factors  $V_{GS}$

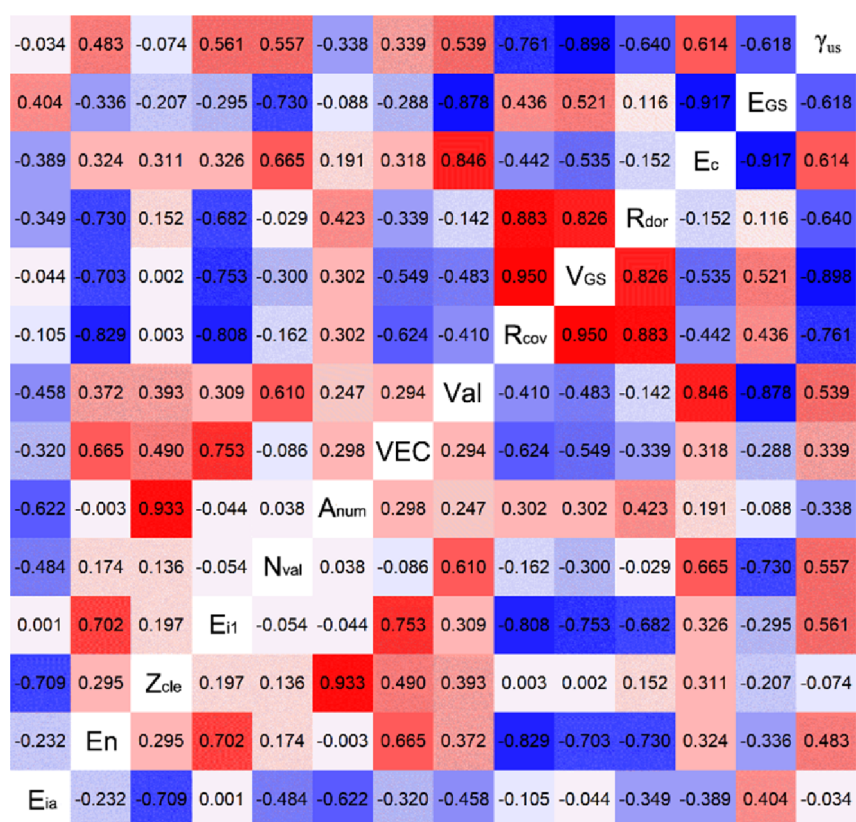


Figure 7. Correlation map between  $\gamma_{us}$  and 13 features of alloying elements.

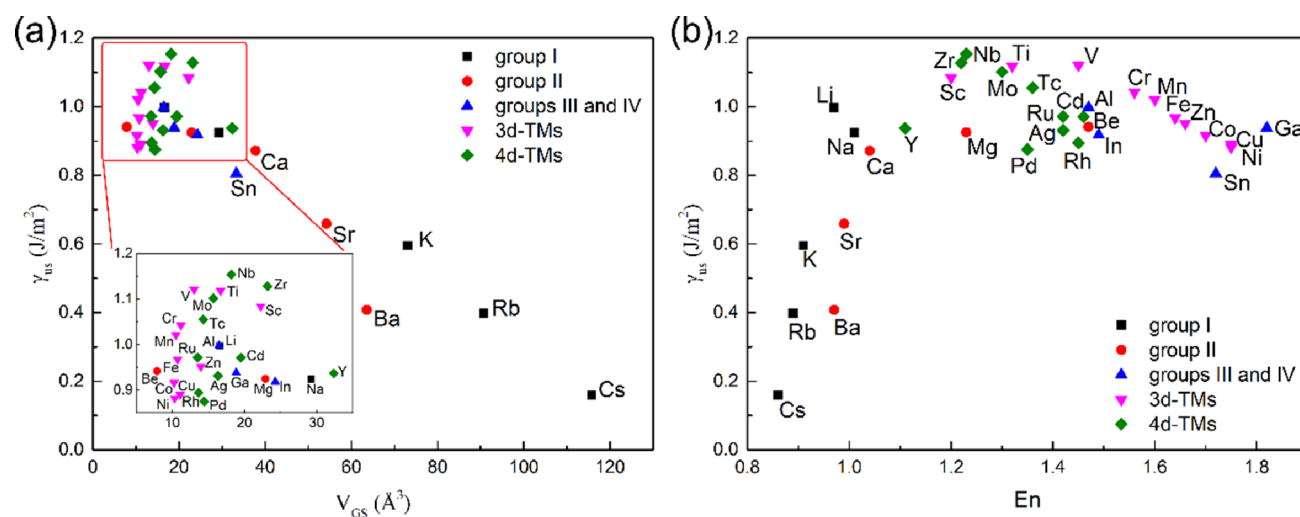
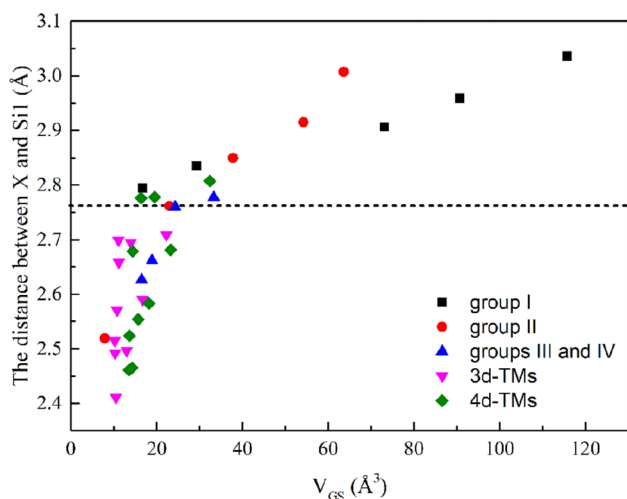


Figure 8. Variation of calculated SFE with respect to (a)  $V_{GS}$  of alloying elements and (b)  $En$  of alloying elements.

is shown in Figure 8a. In general, alloying elements with a larger  $V_{GS}$  would be favorable as alloying element addition reduces SFE in  $Mg_2Si$  alloys. It is worth noting that for transitional elements, the opposite trend is shown. As the  $V_{GS}$  increases,  $\gamma_{us}$  also increases. This may be due to the fact that for alloying elements with  $V_{GS}$  greater than Mg, as the  $V_{GS}$  increases, the distance between the alloying element and Si1 increases (as shown in Figure 9), and the interlayer spacing of the slip plane increases, which, in general, weakens the Si1–Si2 bond, resulting in a decrease in  $\gamma_{us}$ . For alloying elements with  $V_{GS}$  less than Mg, the distance between the alloying element and Si1 is always smaller than the distance between Mg and Si1

in the pure  $Mg_2Si$  system. Such trends are caused by the competition between the size effect and the electronic effect, as shown in Figure 8b. For alloying elements with  $V_{GS}$  less than Mg, as  $En$  increases,  $\gamma_{us}$  decreases. The greater the  $En$  is, the stronger the ability to attract electrons in the compound is, which reduces the electron distribution between Si1 and Si2, weakens the Si1–Si2 bond, and results in a decrease in  $\gamma_{us}$ . However, large  $V_{GS}$  also reduces the  $\gamma_s$  of the  $Mg_2Si$  system, which is not desirable, as shown in Table 1, because it will make the system easier to break. In summary, addition of alloying elements with appropriate  $V_{GS}$  and higher  $En$  (such as In, Cu, Pd, etc.) would exhibit lower  $\gamma_{us}$  and little change in  $\gamma_s$ ,



**Figure 9.** Distance between alloying elements and Si1 in the  $\text{Mg}_2\text{Si}$  system as a function of the  $V_{\text{GS}}$ .

which means that the Mg–Si–X system would yield a better ductility.

### 3. CONCLUSIONS

First-principles calculations in the context of DFT have been carried out to determine the SFE of 33 alloying elements across the periodic table in  $\text{Mg}_2\text{Si}$ . It is found that the addition of alloying elements with various size effect and electronic effect properties led to a large variation of SFE and ductility. Among the properties of alloying elements, the variation of SFE was found to be strongly related to the  $V_{\text{GS}}$  in the size effect. At the same time, the electronic effect will compete with the size effect to have an impact on SFE. An appropriate  $V_{\text{GS}}$  and higher  $E_{\text{n}}$  would reduce the  $\gamma_{\text{us}}$  in the Mg–Si–X system and yield a better ductility. The alloying elements In, Cu, Pd, etc. are identified to be beneficial to the ductility of  $\text{Mg}_2\text{Si}$  alloys. We anticipate that the conclusions and rules obtained in the present work will provide profound guidelines for further alloying design in the promising  $\text{Mg}_2\text{Si}$  alloys with better ductility.

### 4. METHODS

$\text{Mg}_2\text{Si}$  has an FCC structure corresponding to the space group of  $\text{Fm}\bar{3}\text{m}$ . Mg and Si atoms are located at the 4a (0,0,0) and 8c (1/4,1/4,1/4) sites, as shown in Figure 10a. The solute preferred insertion on the Mg site because of the smaller

formation energy.<sup>40</sup> To calculate the solution energies of Mg–Si–X systems, a  $2 \times 2 \times 2$  supercell containing 63 Mg atoms, 32 Si atoms, and 1 single kind of solute element substituting one Mg atom was built.

To study the unstable SFEs, we employed a slab model of the slip system with 18 layers and 4 atoms in each layer (Figure 10b). Although the interaction between stacking fault and solutes can be extended to several close-packed layers, most of the solutes tend to stably aggregate in the faulted region.<sup>18</sup> Therefore, in the cases of Mg–Si–X systems, one Mg atom in the first nearest-neighbor plane with respect to the stacking fault plane was substituted with an X atom, as shown in Figure 10c. A vacuum layer with a 10 Å thickness was introduced into the slab to avoid image interactions. The atomic positions were only allowed to relax along the direction perpendicular to the slipping layers.

In this study, the DFT<sup>41</sup> calculations were performed using the Vienna Ab initio Simulation Package.<sup>42,43</sup> The interaction potential of the core electrons was described using the projector augmented wave method.<sup>44</sup> The generalized gradient approximation with Perdew–Burke–Ernzerhof<sup>45</sup> parameterization for the exchange correction function was adopted. The cutoff energy for the plane wave basis set was 450 eV. The  $k$ -points were meshed by  $2 \times 2 \times 2$  for the calculation of solution energies and  $3 \times 3 \times 1$  for the calculation of SFE.<sup>46</sup> The semicore  $p$  electrons for all of the elements were treated as valence electrons when available.<sup>44,47</sup>

### AUTHOR INFORMATION

#### Corresponding Author

**Haiyou Huang** – Institute for Advanced Materials and Technology, University of Science and Technology Beijing, Beijing 100083, China; [orcid.org/0000-0002-2801-2535](https://orcid.org/0000-0002-2801-2535); Email: [huanghy@mater.ustb.edu.cn](mailto:huanghy@mater.ustb.edu.cn)

#### Authors

**Xinpeng Zhao** – Institute for Advanced Materials and Technology, University of Science and Technology Beijing, Beijing 100083, China

**Keke Song** – School of Mathematics and Physics, University of Science and Technology Beijing, Beijing 100083, China

**Yu Yan** – Institute for Advanced Materials and Technology, University of Science and Technology Beijing, Beijing 100083, China

**Yanjing Su** – Institute for Advanced Materials and Technology, University of Science and Technology Beijing, Beijing 100083, China; Beijing Advanced Innovation Center

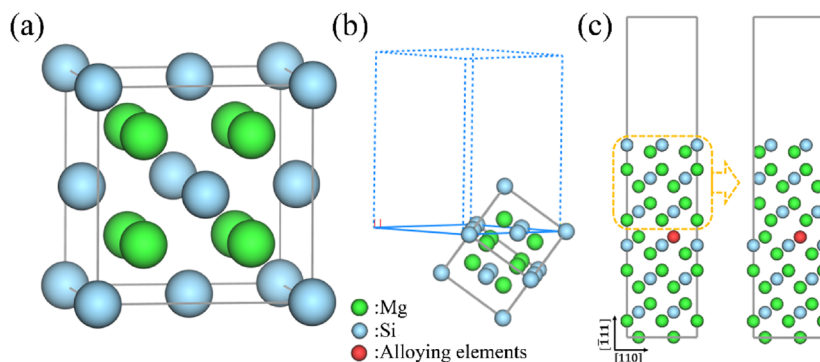


**Figure 10.** (a) Unit cell of  $\text{Mg}_2\text{Si}$ , (b) schematic view of a slab model used for SFE calculations, and (c) displacement of the  $\{111\}\langle 110\rangle$  slip system to explain the formation of the stacking fault. Mg, Si, and alloying elements are colored in green, light blue, and red, respectively.

for Materials Genome Engineering, University of Science and Technology Beijing, Beijing 100083, China; [orcid.org/0000-0003-2773-4015](https://orcid.org/0000-0003-2773-4015)

Ping Qian – School of Mathematics and Physics, University of Science and Technology Beijing, Beijing 100083, China

Complete contact information is available at:

<https://pubs.acs.org/10.1021/acsomega.1c02099>

## Notes

The authors declare no competing financial interest.

## ACKNOWLEDGMENTS

This research was funded by the Guangdong Major Project of Basic and Applied Basic Research (Grant no. 2019B030302011), the National Key Research and Development Program of China (Grant no. 2018YFB0704300), the Guangdong Province Key Area R&D Program (Grant no. 2019B010940001), and the Scientific and Technological Innovation Foundation of Shunde Graduate School, USTB (no. BK19BE030). Also, this work was supported by Xi'an Fengdong Yixiang Technology Service Co., Ltd.

## REFERENCES

- (1) Liu, W.; Tan, X. J.; Yin, K.; Liu, H. J.; Tang, X.; Shi, J.; Zhang, Q.; Uher, C. Convergence of conduction bands as a means of enhancing thermoelectric performance of N-Type  $Mg_2Si_{1-x}Sn_x$  solid solutions. *Phys. Rev. Lett.* **2012**, *108*, No. 166601.
- (2) Jiang, G.; He, J.; Zhu, T.; Fu, C.; Liu, X.; Hu, L.; Zhao, X. High performance  $Mg_2(Si, Sn)$  solid solutions: A point defect chemistry approach to enhancing thermoelectric properties. *Adv. Funct. Mater.* **2014**, *24*, 3776–3781.
- (3) Hirayama, N.; Iida, T.; Funashima, H.; Morioka, S.; Sakamoto, M.; Nishio, K.; Kogo, Y.; Takanashi, Y.; Hamada, N. First-principles study on structural and thermoelectric properties of Al- and Sb-doped  $Mg_2Si$ . *J. Electron. Mater.* **2015**, *44*, 1656–1662.
- (4) Farahi, N.; Prabhudev, S.; Botton, G. A.; Salvador, J. R.; Kleinke, H. Nano- and microstructure engineering: An effective method for creating high efficiency magnesium silicide based thermoelectrics. *ACS Appl. Mater. Interfaces* **2016**, *8*, 34431–34437.
- (5) Mao, J.; Kim, H. S.; Shuai, J.; Liu, Z.; He, R.; Saparamadu, U.; Tian, F.; Liu, W.; Ren, Z. thermoelectric properties of materials near the band crossing line in  $Mg_2Sn$ – $Mg_2Ge$ – $Mg_2Si$  system. *Acta Mater.* **2016**, *103*, 633–642.
- (6) Janot, R.; Cuevas, F.; Latroche, M.; Percheron-Guégan, A. Influence of crystallinity on the structural and hydrogenation properties of  $Mg_2X$  phases ( $X = Ni, Si, Ge, Sn$ ). *Intermetallics* **2006**, *14*, 163–169.
- (7) Udono, H.; Yamanaka, Y.; Uchikoshi, M.; Isshiki, M. Infrared photoreponse from pn-junction  $Mg_2Si$  diodes fabricated by thermal diffusion. *J. Phys. Chem. Solids* **2013**, *74*, 311–314.
- (8) Li, A.; Zhao, X. P.; Huang, H. Y.; Ma, Y.; Gao, L.; Su, Y. J.; Qian, P. Fine-tuning the ductile-brittle transition temperature of  $Mg_2Si$  intermetallic compound via Al doping. *Int. J. Miner., Metall. Mater.* **2019**, *26*, 507–515.
- (9) Wang, Y.; Choo, H. Influence of texture on Hall–Petch relationships in an Mg alloy. *Acta Mater.* **2014**, *81*, 83–97.
- (10) Basu, S.; Dogan, E.; Kondori, B.; Karaman, I.; Benzerger, A. Towards designing anisotropy for ductility enhancement: A theory-driven investigation in Mg-alloys. *Acta Mater.* **2017**, *131*, 349–362.
- (11) Zheng, R.; Bhattacharjee, T.; Shibata, A.; Sasaki, T.; Hono, K.; Joshi, M.; Tsuji, N. Simultaneously enhanced strength and ductility of Mg–Zn–Zr–Ca Alloy with fully recrystallized ultrafine grained structures. *Scr. Mater.* **2017**, *131*, 1–5.
- (12) Mahjoub, R.; Laws, K. J.; Stanford, N.; Ferry, M. General trends between solute segregation tendency and grain boundary character in aluminum-an ab initio study. *Acta Mater.* **2018**, *158*, 257–268.
- (13) Li, G.; Gill, H.; Varin, R. magnesium silicide intermetallic alloys. *Metall. Trans. A* **1993**, *24*, 2383–2391.
- (14) Chen, S.; Qu, X.; Lei, C.; Huang, B. Room temperature mechanical properties of ordered TiAl+La alloys. *Acta Metall. Sin.* **1994**, *30*, 20–24.
- (15) Qi, Y.; Mishra, R. K. Ab initio study of the effect of solute atoms on the stacking fault energy in aluminum. *Phys. Rev. B* **2007**, *75*, No. 224105.
- (16) Wang, C.; Zhang, H. Y.; Wang, H. Y.; Liu, G. J.; Jiang, Q. C. Effects of doping atoms on the generalized stacking-fault energies of Mg alloys from first-principles calculations. *Scr. Mater.* **2013**, *69*, 445–448.
- (17) Zhang, J.; Dou, Y.; Dong, H. Intrinsic ductility of Mg-based binary alloys: A first-principles study. *Scr. Mater.* **2014**, *89*, 13–16.
- (18) Wu, Y.; Li, S.; Ding, Z.; Liu, W.; Zhao, Y.; Zhu, Y. Effect of charge redistribution factor on stacking-fault energies of Mg-based binary alloys. *Scr. Mater.* **2016**, *112*, 101–105.
- (19) Tsuru, T.; Somekawa, H.; Chrzan, D. Interfacial segregation and fracture in Mg-based binary alloys: Experimental and first-principles perspective. *Acta Mater.* **2018**, *151*, 78–86.
- (20) Dong, Q.; Luo, Z.; Zhu, H.; Wang, L.; Ying, T.; Jin, Z.; Li, D.; Ding, W.; Zeng, X. Basal-plane stacking-fault energies of Mg alloys: A first-principles study of metallic alloying effects. *J. Mater. Sci. Technol.* **2018**, *34*, 1773–1780.
- (21) Stanev, V.; Oses, C.; Kusne, A. G.; Rodriguez, E.; Paglione, J.; Curtarolo, S.; Takeuchi, I. Machine learning modeling of superconducting critical temperature. *npj Comput. Mater.* **2018**, *4*, 1–14.
- (22) Pei, Z.; Yin, J.; Hawk, J. A.; Alman, D. E.; Gao, M. C. Machine-learning informed prediction of high-entropy solid solution formation: Beyond the hume-rothery rules. *npj Comput. Mater.* **2020**, *6*, 1–8.
- (23) Kong, X. S.; Wu, X.; You, Y. W.; Liu, C.; Fang, Q.; Chen, J. L.; Luo, G. N.; Wang, Z. First-principles calculations of transition metal–solute interactions with point defects in tungsten. *Acta Mater.* **2014**, *66*, 172–183.
- (24) Tatsuoka, H.; Takagi, N.; Okaya, S.; Sato, Y.; Inaba, T.; Ohishi, T.; Yamamoto, A.; Matsuyama, T.; Kuwabara, H. Microstructures of semiconducting silicide layers grown by novel growth techniques. *Thin Solid Films* **2004**, *461*, 57–62.
- (25) Rice, J. R. Dislocation nucleation from a crack tip: An analysis based on the peierls concept. *J. Mech. Phys. Solids* **1992**, *40*, 239–271.
- (26) Shi, S.; Zhu, L.; Zhang, H.; Sun, Z.; Ahuja, R. Mapping the relationship among composition, stacking fault energy and ductility in Nb alloys: A first-principles study. *Acta Mater.* **2018**, *144*, 853–861.
- (27) Li, A. *Effects of alloy elements on the ductile brittle transition temperature of  $Mg_2Si$* . Master Dissertation, University of Science and Technology Beijing, Beijing, China, 2018. <http://thesis.ustb.edu.cn/docinfo.action?id1=4a4ed95fff89b4a553f4464418cb2d6c&id2=SvYlzbPXJok%253D> (accessed Jul 02, 2020)
- (28) Xu, M.; Cheng, Y.; Sheng, H.; Ma, E. Nature of atomic bonding and atomic structure in the phase-change  $Ge_2Sb_2Te_5$  glass. *Phys. Rev. Lett.* **2009**, *103*, No. 195502.
- (29) Shang, S.; Wang, Y.; Du, Y.; Tschoopp, M. A.; Liu, Z. K. Integrating computational modeling and first-principles calculations to predict stacking fault energy of dilute multicomponent Ni-base alloys. *Comput. Mater. Sci.* **2014**, *91*, 50–55.
- (30) Achmad, T. L.; Fu, W.; Chen, H.; Zhang, C.; Yang, Z. G. Co-based alloys design based on first-principles calculations: Influence of transition metal and rare-earth alloying element on stacking fault energy. *AIP Conf. Proc.* **2017**, *1805*, No. 060004.
- (31) Webelements. <http://www.webelements.com> (accessed Feb 07, 2020).
- (32) Pauling File. <http://www.paulingfile.com/> (accessed Feb 07, 2020).
- (33) Ward, L.; Agrawal, A.; Choudhary, A.; Wolverton, C. A general-purpose machine learning framework for predicting properties of inorganic materials. *npj Comput. Mater.* **2016**, *2*, 1–7.
- (34) Periodictable. <https://www.periodictable.com/> (accessed Feb 07, 2020).
- (35) Breiman, L. Random forests. *Mach. Learn.* **2001**, *45*, 5–32.

- (36) Svetnik, V.; Liaw, A.; Tong, C.; Culberson, J. C.; Sheridan, R. P.; Feuston, B. P. Random forest: A classification and regression tool for compound classification and qsar modeling. *J. Chem. Inf. Model.* **2003**, *43*, 1947–1958.
- (37) Loh, W. Y. Fifty years of classification and regression trees. *Int. Stat. Rev.* **2014**, *82*, 329–348.
- (38) Loh, W. Y. Classification and regression trees. *Wiley Interdiscip. Rev.: Data Min. Knowl.* **2011**, *1*, 14–23.
- (39) Cutler, A.; Cutler, D. R.; Stevens, J. R. Random forests. In *Ensemble Machine Learning*; Springer: Boston, MA, 2012, pp 157–175.
- (40) Tani, J. I.; Kido, H. First-principles and experimental studies of impurity doping into Mg<sub>2</sub>Si. *Intermetallics* **2008**, *16*, 418–423.
- (41) Kohn, W.; Sham, L. J. Self-consistent equations including exchange and correlation effects. *Phys. Rev.* **1965**, *140*, No. A1133.
- (42) Kresse, G.; Hafner, J. Ab initio molecular dynamics for open-shell transition metals. *Phys. Rev. B* **1993**, *48*, No. 13115.
- (43) Kresse, G.; Furthmüller, J. Efficient iterative schemes for ab initio total-energy calculations using a plane-wave basis set. *Phys. Rev. B* **1996**, *54*, No. 11169.
- (44) Blöchl, P. E. Projector augmented-wave method. *Phys. Rev. B* **1994**, *50*, No. 17953.
- (45) Perdew, J. P.; Burke, K.; Ernzerhof, M. Generalized gradient approximation made simple. *Phys. Rev. Lett.* **1996**, *77*, No. 3865.
- (46) Monkhorst, H. J.; Pack, J. D. Special points for brillouin-zone integrations. *Phys. Rev. B* **1976**, *13*, No. 5188.
- (47) Kresse, G.; Joubert, D. From ultrasoft pseudopotentials to the projector augmented-wave method. *Phys. Rev. B* **1999**, *59*, No. 1758.